NUCLEAR TECHNOLOGY
© 2025 The Author(s). Published with license by Taylor & Francis Group, LLC.
DOI: https://doi.org/10.1080/00295450.2025.2521972

Check for updates

Fuel and Graphite Temperatures in a Micro Nuclear Reactor During a DLOFC

Charl du Toit,[a]* Wayne Boyes,[b] and Johan Slabber[b]

[a]North-West University, Unit for Energy and Technology Systems, Potchefstroom, South Africa
[b]University of Pretoria, Department of Mechanical and Aeronautical Engineering, Pretoria, South Africa

Received April 7, 2025
Accepted for Publication June 8, 2025

Abstract — *The Advanced Micro Reactor (AMR), a high-temperature gas-cooled prismatic block reactor, is being designed to produce 10 MW of thermal power. The active core consists of an inner graphite reflector, fuel graphite block assemblies arranged in three rings, and an outer graphite reflector (OR). The system code Flownex SE has been used to set up an axisymmetric network model of the reactor to study the thermal-hydraulic behavior of the reactor under steady-state conditions and during a depressurized loss-of-forced cooling (DLOFC) event.*

The helium coolant enters the reactor at 320°C, flows up in the risers in the OR to the upper plenum, down through the core, and exists the lower plenum at 750°C. In the risers, the coolant is preheated to 324.8°C. Under steady-state conditions, the top of the core is on average 403°C cooler than the bottom of the core, and the maximum fuel and graphite temperatures are 1032.4°C and 809.0°C, respectively.

During the DLOFC, the reactor endeavors to heat up the upper part of the core, cool down the lower part of the core, and set up the required temperature gradient in the radial direction to remove the decay heat and the excess heat accumulated in the solids. When the DLOFC starts and the reactor is scrammed, the fuel temperatures drop steeply, along with the drop in power, until they are in equilibrium with the corresponding graphite temperatures, and then follow the graphite temperatures as the decay heat decreases and the graphite heats up or cools down.

This paper focuses among other things on the accumulation and release of heat by the fuel and solids during the DLOFC. The thermal behavior of the inner ring of the fuel block assemblies receives special attention.

Keywords — *Prismatic block reactor, gas-cooled reactor, steady-state temperatures, DLOFC heat accumulation rates.*

Note — *Some figures may be in color only in the electronic version.*

I. INTRODUCTION

The Advanced Micro Reactor (AMR) is a high-temperature gas-cooled prismatic block reactor under design to produce 10 MW of thermal power.[1] The active core consists of 24 fuel graphite block assemblies arranged in three rings, and 19 control rod (CR) graphite block assemblies. Each assembly consists of three graphite blocks stacked lengthwise. The central inner reflector (IR) is formed by a CR graphite block assembly, and the core is enclosed by an outer reflector (OR). The core contains 1260 fuel assemblies (FAs) each consisting of a silicon-carbide (SiC) tube housing low-enriched TRISO-coated particle fuel immersed in a lead-bismuth eutectic alloy (LBE). The FAs and CRs are placed in borings that line up vertically in the graphite moderator blocks, allowing annuli for the helium coolant flow.

*Email: jat.dutoit@nwu.ac.za
This is an Open Access article distributed under the terms of the Creative Commons Attribution-NonCommercial-NoDerivatives License (http://creativecommons.org/licenses/by-nc-nd/4.0/), which permits non-commercial re-use, distribution, and reproduction in any medium, provided the original work is properly cited, and is not altered, transformed, or built upon in any way. The terms on which this article has been published allow the posting of the Accepted Manuscript in a repository by the author(s) or with their consent.

Although detailed computational fluid dynamic (CFD) models can be set up of a prismatic block reactor to simulate the flow and heat transfer,[2,3] the computational resources required often preclude the simulation of the full reactor and the associated thermal flow systems. However, system network codes are suited to study the thermal-fluid performance of reactor systems and can provide valuable insights. Maruyama et al.[4] used the flow network analysis code FLOWNET in association the fuel temperature analysis code TEMDIM to evaluate the core thermal and hydraulic characteristics of the high temperature test reactor (HTTR). They performed steady-state simulations at selected stages during the fuel cycle.

Rousseau and Greyvenstein[5] also simulated the HTTR employing the network code Flownet (later to become Flownex SE) and determined the graphite and fuel temperatures for a chosen steady-state condition. By coupling the thermal-hydraulic systems code RELAP5-3D to the CFD code Fluent, Anderson et al.[6] modeled the flow in the core and the mixing in the outlet plenum of a very-high-temperature reactor (VHTR).

Kim et al.[7] employed the systems code GAMMA+ to assess design options for reactor vessel cooling in the PMR-600 prismatic core VHTR. The network model also accounted for the core and the reactor cavity cooling system (RCCS). A network model of the core structures and the associated RCCS of the PMR-200 prismatic core VHTR was constructed by Nel[8] using the system code Flownex SE.[9] He performed an analysis of the thermal-hydraulic behavior for a typical steady-state condition. In the current study a two-dimensional (2D) axisymmetric network model has been set up of the AMR using the system code Flownex SE.[9]

Apart from the modeling of the thermal flow behavior of the reactor under steady-state conditions, the modeling of the thermal flow behavior during a depressurized loss-of–forced cooling (DLOFC) is of importance when all the pressurized coolant is lost due to a pipe break. Under these conditions, the reactor must rely solely on conduction and radiation and convection heat transfer to the surrounding environment to cool down the reactor passively. Typically, the maximum fuel, reactor pressure vessel (RPV), core barrel (CB), and graphite temperatures are of interest.[7,10,11] However, a thorough evaluation of the underlying phenomena is required to understand the thermal flow behavior of the reactor resulting in the temperature variations.

The purpose of this paper is to use the current conceptual design of the AMR to demonstrate the application of a methodology to study the heating and cooling of the core by focusing, in particular, on the inner fuel ring to understand and evaluate how heating and cooling develop with time and the relationship between the fuel and graphite temperatures during a DLOFC. The methodology also helps with the identification of the underlying phenomena that determine the behavior of the reactor during a DLOFC.

II. FLOWNEX MODEL OF THE AMR

A cut view through the AMR is shown in Fig. 1. The upper and lower domes shown in Fig. 1 were not included in the Flownex model. Considering the fact that there is no primary flow occurring in the upper and lower domes and that the domes are shielded from the core by the upper and bottom structures, it was assumed that their contributions to the thermal flow would be small. However, once the information of a more detailed design is available, the domes will be included in the model.

In the axial direction, the reactor was discretized into 12 increments: (1) top reflector (TR), (2) upper plenum (UP), (3) to (9) seven core layers (I through VII), with the first and last being a quarter fuel block high and the others half of a block high comprising the three layers of fueled graphite blocks, (10) bottom reflector (BR), (11) lower plenum (LP), and (12) bottom support (BS).

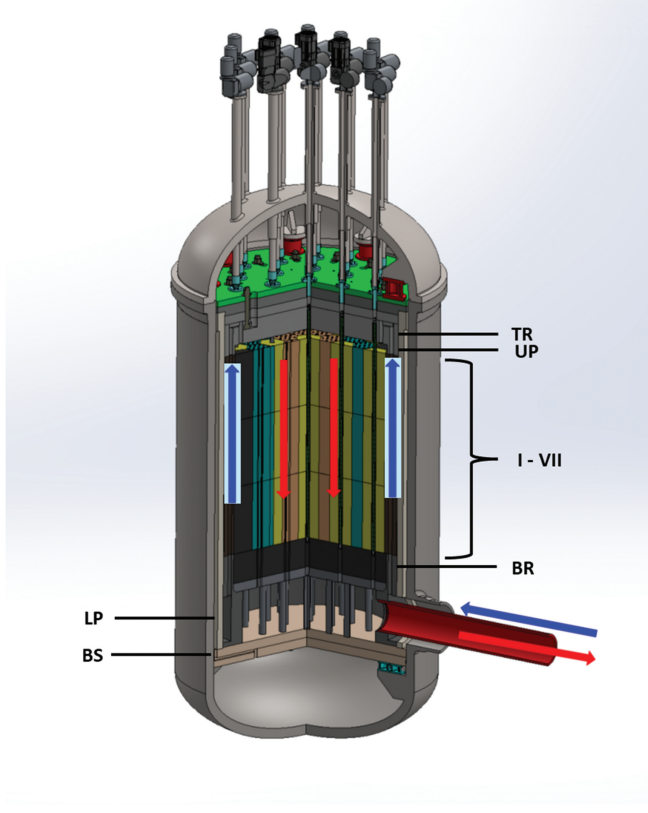

Fig. 1. Cut view through the AMR.

Figure 2 shows a cross section through the AMR core. In the radial direction, as indicated in Fig. 2, the reactor has been discretized into 11 rings: (1) IR + CR, (2) first fuel ring (FU) (graphite 1 + FU1), (3) second FU (graphite 2 + FU2 + CR), (4) third FU (graphite 3 + FU3 + CR), (5) OR + CR + risers, (6) gap between the OR and CB, (7) CB, (8) gap between the CB and RPV, (9) RPV, (10) cavity between the RPV and RCCS, and (11) RCCS face plate.

The IR, fuel FA blocks, and OR are assumed to fit tightly, and thus no cross flow, bypass gaps between the blocks, or contact thermal conductance between the blocks were accounted for. However, once the information for a more detailed design is available, the cross flow and bypass gaps, as well as the contact thermal conductance between the blocks, will be included in the model.

The Flownex network model consists of collections of one-dimensional components and fluid and solid nodes or control volumes (CVs). The flow components account for the conservation of momentum and the advective transport of energy between the fluid nodes. The fluid and solid nodes account for the conservation of mass and energy.

Pipe components were used to model the flow in the risers, plenums, coolant channels, and the inlet and outlet pipes. The convection heat transfer between the solids and the gas was modeled using convection components. Conduction components were used to model the heat conduction heat transfer through the solids. Finally, radiation heat transfer components were used to model the radiation heat transfer across the annuli between the CR and FA tubes and the graphite, between the OR and the CB, between the CB and the RPV, and between the RPV and RCCS face plate. The helium in the gaps between the OR and CB, and the CB and RPV were assumed to be stagnant, and conduction through the helium was also considered. For each ring of graphite blocks, only a representative CR, a representative FA, a representative coolant channel, and a representative riser channel, as applicable, were modeled.[8]

The Flownex network model consisted of three interconnected networks. The first network modeled the graphite blocks, CB, RPV wall, reactor cavity, and RCCS face plate. The network also accounted for the radiation and conduction across the gaps between the OR and CB, and the CB and RPV, as well as the radiation and convection across the cavity between the RPV and RCCS. The second network modeled the flow paths, CRs, and the SiC tubes of the FAs. The network also accounted for the radiation heat transfer across the annuli and the convection heat transfer in the annuli and the risers. The third network modeled the conduction through the coated particle fuel and LBE mix inside the SiC tubes. The power that was generated by the fuel was distributed between the CVs in the network. The details of the layouts of the networks can be found in Boyes et al.[1]

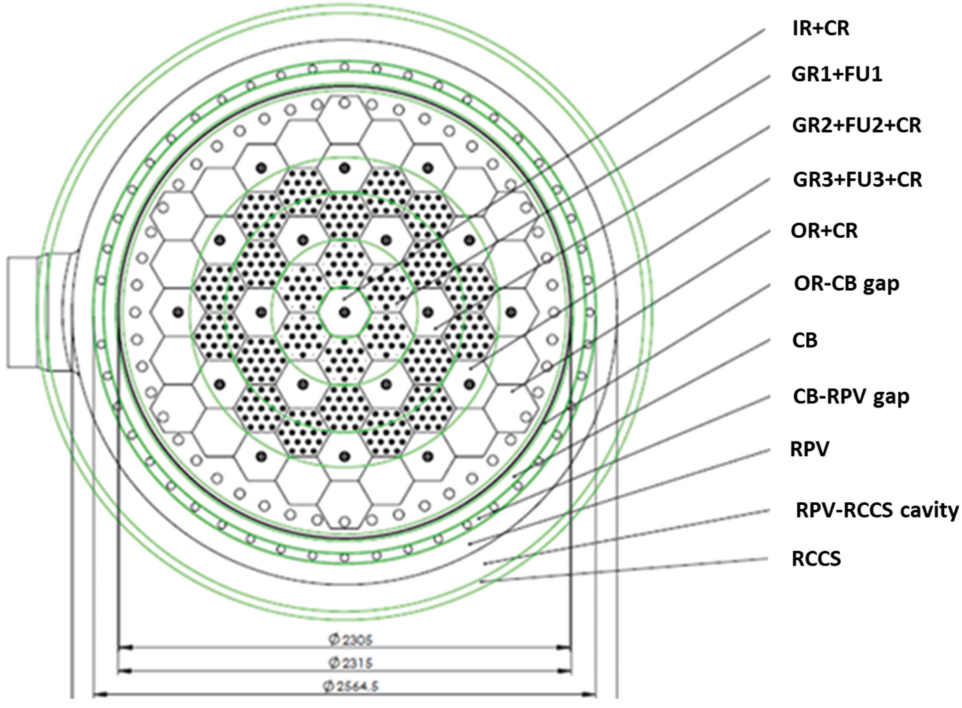

Fig. 2. Cross section through the AMR core.

The equation for the conservation of mass for the flow node i is given as[9]

$$\frac{\partial}{\partial t}(\rho V_i) = \sum \dot{m}_{in} - \sum \dot{m}_{ex} + d_i \quad . \tag{1}$$

When gravitational effects are neglected, the equation for the conservation of momentum for the pipe component connecting two flow nodes can be expressed as[9]

$$\begin{aligned} &\frac{L_i}{A_i}\frac{\partial}{\partial t}(\dot{m}) + (p_{0,ex} - p_{0,in}) \\ &\quad + \left[\left(\frac{f_i L_i}{D_{H,i}} + K\right) \cdot \frac{|\dot{m}|\dot{m}}{2\overline{\rho}_i A_i^2}\right] \\ &\quad = 0 \quad . \end{aligned} \tag{2}$$

The friction factor f is calculated using an explicit version of the Colebrooke-White correlation.[12]

The equation for the conservation of energy for flow node i is given as[9]

$$\begin{aligned} \frac{\partial}{\partial t}(m_i h_{0,i}) - V_i \frac{\partial p_i}{\partial t} = &\sum_{in,j} \left[\dot{m}_j h_{0,j} + \dot{Q}_j\right] \\ &+ d_i^+ h_{0,amb} \\ &- (h_{0,i})\left(\sum_{ex,j} \dot{m}_j + d_i^-\right) \\ &+ \dot{Q}_i \ , \end{aligned} \tag{3}$$

where the first term on the right side is the energy of the fluid flowing in from the adjacent flow nodes, the second term is the energy added by any mass source, and the third term is energy that flows out to adjacent flow nodes and is associated with any mass sink. $\dot{Q}_j$ is any energy added to the inflowing fluid between two adjacent flow nodes, and $\dot{Q}_i$ is any energy added directly to the flow node; both can include convection heat transfer.

The equation for the conservation of energy for a solid node is given as[9]

$$\frac{\partial}{\partial t}(m_i c_{p,i} T_{0,i}) = -\sum \dot{q}_{conv} + \sum \dot{q}_{cond} + \sum \dot{q}_{rad} + \dot{Q}_i \, . \tag{4}$$

The convection heat transfer from the solids to the fluid in a pipe component was obtained using[9]

$$\dot{q}_{conv} = -h_i A_i (T_f - T_s) \quad . \tag{5}$$

The heat transfer coefficient h was obtained from the Nusselt number, which was calculated using the Gnielinski correlation.[13]

The conduction heat transfer through the solids was calculated using[9]

$$\dot{q}_{cond} = -\frac{k_s A_i}{L_{ij}}(T_i - T_j) \quad . \tag{6}$$

The radiation heat transfer across the gaps was obtained by employing the surface-to-surface radiation component using[9]

$$\dot{q}_{rad} = -\left[\sigma\left(T_i^4 - T_j^4\right)\right] / \left[\frac{1-\varepsilon_i}{\varepsilon_i A_i} + \frac{1}{A_i F_{ij}} + \frac{1-\varepsilon_j}{\varepsilon_j A_j}\right] \quad . \tag{7}$$

The view factor between the inner and outer surfaces of the annular gaps was taken as $F_{ij} = 1$.[13] Under steady-state conditions, helium enters the cold inlet (blue arrow in Fig. 1) at a flow rate of 4.442 kg/s and a temperature of 320°C. The helium moves up through the risers into the UP, as indicated in Fig. 1, where it is distributed between the annuli around the CRs and FAs. The helium flows down through the core, as indicated in Fig. 1, where it collects heat, through the holes in the BR into the LP, and then exits the hot outlet (red arrow in Fig. 1) at a temperature of 750°C and a pressure of 4 MPa.

The inlet and outlet temperatures and outlet pressure are design variables, and the mass flow rate was determined iteratively to ensure the required temperature rise over the reactor accounting also for the RCCS heat, losses. The temperature at the outer surface of the RCCS face plate was prescribed as 65°C.[10,11] The emissivities of the CB, RPV, and RCCS, which were adopted from Rousseau et al.[14] and were assumed to be 0.8 with the associated convection heat transfer coefficients being 4.0 W/m^{2}K.

No neutronics calculations were performed, but the relevant values of the power were applied directly to the nodes of the fuel elements. The decay power $\dot{Q}_{DH}$ was modeled employing the Wigner-Way correlation[15] given by

$$\begin{aligned} \dot{Q}_{DH}(t) = &\dot{Q}_0 \times 0.06 \\ &\times \left[(t - t_1)^{-0.2} - (t - t_1 + t_s)^{-0.2}\right] \end{aligned} \tag{8}$$

where $\dot{Q}_0 = 10^6$ W is the nominal power, $t_1 = 5$s is the time at which the reactor was shut down or scrammed,

and $t_s = 15$years expressed in seconds is the time of operation before the start of the DLOFC event.

The power generated in the fuel under steady-state and transient conditions was distributed in the axial direction according to a sine profile. During the DLOFC, the transient variation of the coolant mass flow rate $\dot{m}$ at the inlet after the scram was modeled to have a cosine variation to avoid numerical instabilities at the start and end times of the duration,

$$\dot{m}(t) = \dot{m}_\infty + \left(\frac{\dot{m}_0 - \dot{m}_\infty}{2}\right) \times \left(cos\left(\pi\left(\frac{t - t_1}{t_2 - t_1}\right)\right) + 1\right) \quad , \tag{9}$$

where $t_2 = 10$s is the time when the mass flow rate transient ends, $\dot{m}_\infty = 0.1$mg/s is the assumed ultimate residual mass flow rate, and $\dot{m}_0 = 4.442$kg/s is the nominal mass flow rate, as mentioned previously.

The transient variation of the outlet total pressure p_0 after the scram was also modeled to have a cosine variation to avoid numerical instabilities at the start and end times of the duration,

$$p_0(t) = p_{0\infty} + \left(\frac{p_{00} - p_{0\infty}}{2}\right) \times \left(cos\left(\pi\left(\frac{t - t_1}{t_2 - t_1}\right)\right) + 1\right) \quad , \tag{10}$$

where $p_{0\infty} = 103$kPa is the ultimate total pressure, assumed to be the atmospheric pressure, and $p_{00} = 4$MPa is the nominal total pressure, as mentioned before.

Flownex SE employs a finite volume–based iterative implicit pressure correction method[16] to obtain the steady-state solution of the conservation equations. The finite volume–based noniterative algorithm implemented in Flownex SE was employed to obtain the transient solution of the conservation equations. The transient solution was run for 5 s with fixed boundary conditions. It was assumed that the DLOFC (pipe break) and the scram of the reactor occurred simultaneously at 5 s. Equations (8), (9), and (10) were then activated at that instant. The initial time step was specified as 5 ms. After 35 s, the time step was gradually increased until it reached 5000 s at 50 min.

Du Toit[17] demonstrated the validity of the modeling approach used in this study by comparing the results obtained for the flow and heat transfer in a prismatic fuel block and a prismatic fuel block assembly, with the corresponding results obtained from more detailed CFD simulations.

III. RESULTS

Three sets of results are presented. First, the temperature distribution in the reactor under steady-state conditions is considered. Second, the variations in the graphite and fuel temperatures of the fuel graphite block assemblies during the initial 20 h of the DLOFC are presented. Last, the heating/cooling rates of the reactor core (IR to OR radially and core layer I to BR axially) at selected time instances are discussed.

III.A. Steady-State Temperatures

The temperature distribution in the reactor under steady-state conditions is shown in Fig. 3. The IR and

	IR	GR1	FU1	GR2	FU2	GR3	FU3	OR	ORo	CBi	CBo	RPVi	RPVo
TR	329.9	329.9		329.8		329.7		329.5	324.7	300.4	291.1	219.2	213.2
UP								341.8	336.8	311.7	300.9	223.2	216.8
I	368.3	360.7	406.0	360.8	405.9	358.5	404.9	345.7	339.2	313.8	302.8	224.1	217.7
II	421.4	424.0	605.0	421.9	603.4	415.9	599.3	357.8	351.0	325.0	313.5	231.7	224.7
III	520.1	537.9	836.7	531.6	832.6	517.6	823.4	373.6	366.0	338.0	325.4	239.8	232.2
IV	628.9	665.3	988.8	653.5	981.3	629.7	965.8	388.3	379.7	349.8	336.2	247.1	238.9
V	714.9	764.9	1032.4	747.8	1020.9	714.6	998.4	397.1	388.0	356.9	342.8	251.6	243.1
VI	759.5	809.0	962.5	788.4	947.3	747.0	916.9	397.9	388.8	357.7	343.6	252.4	243.9
VII	774.7	801.6	855.9	774.9	837.2	711.6	797.3	391.4	382.5	352.8	339.1	249.9	241.6
BR	724.6	795.3		764.0		705.4		386.2	378.6	347.6	333.9	245.1	237.1
LP								365.4	360.4	334.5	322.6	240.2	232.8
BS	389.4	388.6		385.3		379.5		369.4	362.4	335.1	322.9	239.4	231.9
T_ave	614.1	644.8		630.3		600.0		370.3	363.2	335.3	322.9	238.6	231.2
Taj-Tai		-30.8		14.5		30.3		220.3	7.2	27.9	12.4	84.3	7.5

Fig. 3. Steady-state temperatures (°C) in the AMR.

OR temperatures are at the centers of the IRs and ORs, while the ORo, CBi, CBo, RPVi, and RPVo temperatures are the temperatures at the inner (i) and outer (o) surfaces of the OR, CB, and RPV. The temperatures (graphite and FU) are the temperatures of the graphite and at the centers of the FAs for the three rings of fuel graphite block assemblies. The average temperatures T_ave are the average temperatures of core layer I to the BR for the IR, graphite of ring 1, graphite of ring 2, and graphite of ring 3, and the average temperatures of the TR to the BS for the OR, CB, and RPV. The temperature difference (Taj-Tai) is the difference between the average temperature for a radial position and the average temperature of the previous radial position.

It can be observed in Fig. 3 that the maximum fuel temperature was 1032.4°C and the maximum graphite temperature was 809.0°C, both of which occurred in the first ring of fuel graphite block assemblies. The maximum fuel temperatures of the second and third fuel graphite block assemblies were 1020.9°C and 998.4°C, respectively. The maximum temperatures for the OR, CB, and RPV were 397.9°C, 357.7°C, and 252.4°C, respectively. From the IR to the third fuel graphite block assembly ring, the graphite temperatures increased on average by 403°C from the top of the core (I) to the bottom of the core (VII). Except for the top CV (I), the temperatures of the IR were lower than the temperatures of the inner fuel block assembly ring. This is because no heat is generated in the IR and the heat removed by the coolant flowing around the CR in the IR therefore must be transferred from the inner fuel graphite block assembly ring to the IR.

From the first fuel graphite block assembly ring to the second fuel graphite block assembly ring, the average temperature drop was 14.5°C, from the second fuel graphite block assembly ring to the third fuel graphite block assembly ring the average temperature drop was 30.3°C, and from the third fuel graphite block assembly ring to the OR the average temperature drop was 220.3°C. Because no heat is generated in the OR, the latter large temperature drop is to enable heat to be transferred from the third fuel graphite block assembly ring to the OR, which the OR then primarily transfers to the coolant flowing up from the inlet to the UP in the riser channels in the OR.

It was found that 618.5 kW is transferred to the coolant and that the coolant is preheated from 320.0°C to 346.8°C. The average temperature drop across the gap between the OR and CB was 27.9°C, while the average temperature drop across the gap between the CB and the RPV was 84.3°C. Under steady-state conditions, the RPV transfers 86.1 kW to the RCCS.

When the DLOFC occurred, and the reactor was scrammed, the heat removed by the coolant became negligible after 5 s into the DLOFC. All the decay heat generated and the excess heat accumulated in the solids must be removed via the RCCS. The reactor endeavors to heat up the upper part of the reactor (core), cool down the lower part of the reactor (core), and to set up the appropriate radial temperature gradient for the heat removal. The IR, OR, CB, and RPV must also initially be heated up. Once the desired temperature gradients have been attained, the reactor will have reached a full cooldown mode in which the remaining accumulated heat in the solids and the decay power being generated are rejected via the RCCS. Du Toit et al.[18] have found that the reactor reached a full cooldown mode, that is all the solid CVs are releasing heat, 18 h after the start of the DLOFC.

Thus, in this study only the first 20 h of the DLOFC are considered. In the next subsection, the relationship between the graphite and fuel temperatures of the fuel graphite block assembly rings is studied.

III.B. Fuel and Graphite Temperatures During DLOFC

The variations in the temperatures with time of the seven central CVs of the FAs for the first fuel graphite block assembly ring during the first 20 h of the DLOFC are shown Fig. 4. Similarly, Fig. 5 depicts the variations in the temperatures with time of the corresponding seven CVs of the graphite for the first fuel graphite block assembly ring during the first 20 h of the DLOFC.

It can be seen in Fig. 4 that the temperatures of fuel CVs I, II, and III initially decreased, then increased to peak, and after that continued to decrease. The temperatures of fuel CVs IV, V, VI, and VII continued to decrease. In Fig. 5, it can be observed that the temperatures of graphite CVs I, II, III, IV, V, and VI also initially decreased, then increased to peak, and finally continued to decrease. The temperature of graphite CV VII continued to decrease.

A summary of the steady-state fuel and graphite temperatures of the CVs, the initial minima, the subsequent maxima, and the corresponding times at which they occurred, are given in Table I. It can be observed in Table I there was an initial slight drop in the temperatures of graphite CVs I to VI and that the minima occurred between 8.850 s and 9.905 s. During the initial 5 s of the DLOFC transient, when the decay heat generated dropped sharply, the heat transferred to the coolant flowing through the core was taken from the graphite surrounding the coolant annuli. During this period, the inlet

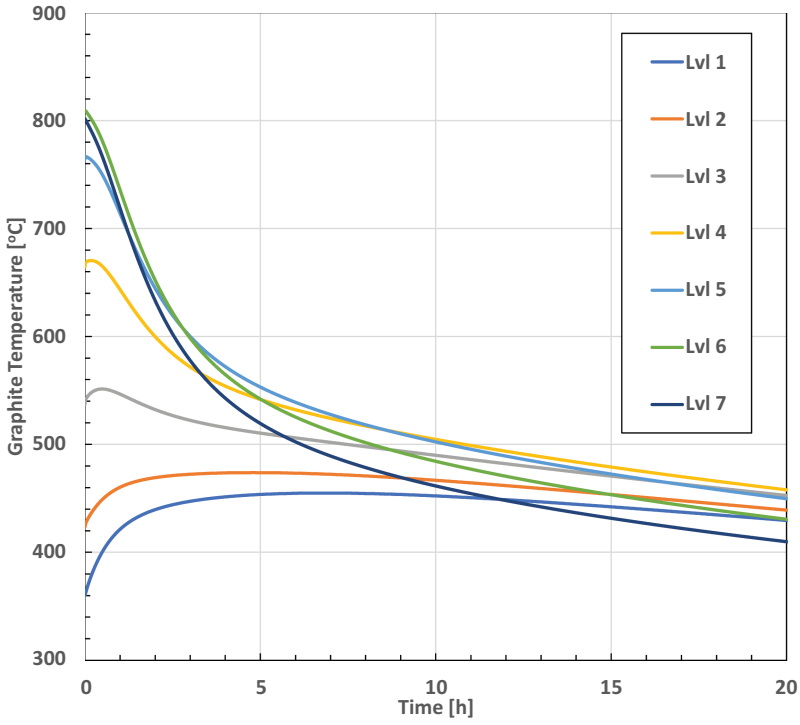

Fig. 4. Variations in the central fuel temperatures of the first fuel block assembly ring of the AMR.

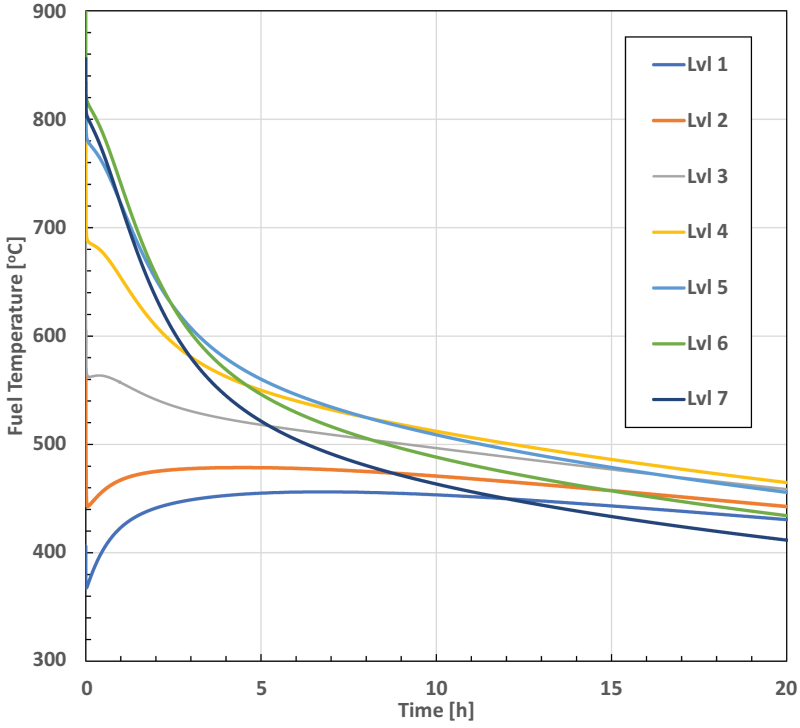

Fig. 5. Variations in the central graphite temperatures of the first fuel block assembly ring of the AMR.

TABLE I

Fuel and Graphite Temperatures of First Ring of Fuel Blocks of the AMR

	Fuel 1					Graphite 1				
	T_0 (°C)	T_{min} (°C)	t_{min} (s)	T_{max} (°C)	t_{max} (s)	T_0 (°C)	T_{min} (°C)	t_{min} (s)	T_{max} (°C)	t_{max} (°C)
I	406.0	367.3	13.0	456.3	24282.0	360.7	360.1	9.91	455.0	24517.0
II	604.9	443.0	197.0	478.7	16102.0	424.0	423.6	9.30	473.9	17262.0
III	836.7	562.4	390.0	563.6	1364.0	537.9	537.4	8.95	551.3	1750.0
IV	988.7	Continue decreasing				665.3	664.8	8.86	670.3	629.0
V	1032.3	Continue decreasing				764.8	764.3	8.86	766.5	94.2
VI	962.5	Continue decreasing				808.9	808.5	8.95	809.2	38.2
VII	855.8	Continue decreasing				801.6	Continue decreasing			

mass flow rate decreased from 4.442 kg/s to 0.1 mg/s, and the outlet pressure dropped from 4000 to 103 kPa.

The drop in pressure initially led to an increase in the mass flow rate through the core and a drop in the temperature of the coolant due to the expansion of the coolant. This also led to an initial increase in the rate at which the heat was transferred from the solids to the coolant before decreasing to finally become negligible. The slight drop in the graphite temperatures was the result of this transfer of heat from the solids to the coolant. It can further be observed that the maximum graphite temperatures of CVs I to VI were all higher than the corresponding steady-state temperatures.

The farther the CV was from the top of the core, the smaller the difference between the maximum DLOFC temperature and the steady-state temperature, and the shorter the time required to reach the maximum DLOFC temperature. The heating/cooling of the graphite CVs is a combination of the axial and radial conduction of heat and the rate at which decay heat is generated. The rate at which decay heat is generated decreased continually.

It is also observed in Table I that the times at which the initial minimum temperatures of fuel CVs I, II, and III occurred were not related to the corresponding times when the minimum graphite temperatures occurred. The drop from the steady-state fuel temperatures to the initial minimum fuel temperatures was also significant. The time when the fuel temperatures reached their minimum values were determined by the required temperature difference between the fuel and graphite temperatures to transfer the decay heat generated at that instant in time from the fuel to the graphite.

After reaching the minimum values, the fuel temperatures followed the graphite temperatures, as can be seen in Figs. 4 and 5, while the decay heat generated steadily decreased. The steady decrease in the decay heat generated led to the fuel temperature for a specific CV reaching its maximum before the corresponding graphite temperature reached its maximum.

Table II provides a summary of the steady-state fuel and graphite temperatures of the CVs, the initial minima, the subsequent maxima, and the corresponding times at which they occurred for the second ring of fuel graphite block assemblies. The corresponding summary of the steady-state fuel and graphite temperatures of the CVs, the initial minima, the subsequent maxima, and the corresponding times at which they occurred for the third ring of fuel graphite block assemblies is given in Table III.

In Table II, it can be seen that for the second of the fuel graphite block assemblies, in the case of the graphite CVs I to VI, there was also a slight drop in temperature between 8.91 s and 9.88 s. However, in the case of the third fuel graphite block assemblies, between 9.19 s and 9.90 s, only the temperatures of CVs I to V dropped slightly. In the second ring of the fuel graphite block assemblies, CVs III to VI reached their maximum graphite temperatures earlier than the corresponding CVs in the first ring of fuel block assemblies reached their maximum graphite temperatures. In the case of the third ring of fuel graphite block assemblies, CVs III to V reached their maximum graphite temperatures earlier than the corresponding CVs in the first and second rings of fuel block assemblies reached their maximum graphite temperatures.

In contrast, in the second ring of fuel graphite block assemblies, CVs I and II reached their maximum graphite temperatures later than the corresponding CVs in the first ring of fuel block assemblies reached their maximum graphite temperatures. Also, in the case of the third ring of fuel

TABLE II

Fuel and Graphite Temperatures of Second Ring of Fuel Blocks of the AMR

	Fuel 2					Graphite 2				
	T_0 (°C)	T_{min} (°C)	t_{min} (s)	T_{max} (°C)	t_{max} (s)	T_0 (°C)	T_{min} (°C)	t_{min} (s)	T_{max} (°C)	t_{max} (°C)
I	405.9	368.0	85.5	445.7	26477.0	360.8	360.5	9.88	444.4	26712.0
II	603.4	439.5	248.0	467.4	19542.0	421.9	421.6	9.26	462.7	20437.0
III	832.6	Continue decreasing				531.6	531.3	8.97	536.3	540.0
IV	981.3	Continue decreasing				653.5	653.1	8.91	655.4	207.0
V	1020.9	Continue decreasing				747.8	747.4	8.94	748.4	46.6
VI	947.3	Continue decreasing				788.4	788.0	9.10	788.2	23.5
VII	837.2	Continue decreasing				774.9	Continue decreasing			

graphite block assemblies, CVs I and II reached their maximum graphite temperatures later than the corresponding CVs in the first and second rings of the fuel block assemblies reached their maximum graphite temperatures.

Further, it can be observed that for both the second ring of fuel graphite block assemblies for CVs I to V and the third ring of fuel graphite block assemblies for CVs I to VI, the maximum graphite temperatures were all higher than the corresponding steady-state temperatures. However, in the case of the second ring of fuel graphite block assemblies, the maximum temperature of CV VI, and in the case of the third ring of fuel graphite block assemblies, the maximum temperature of CV V, were slightly lower than the corresponding maximum steady-state temperatures.

It can be observed in Tables II and III that only the fuel temperatures for CVs I and II for both the second and third rings of fuel graphite block assemblies decreased to an initial minimum, then increased to a maximum before continuing to decrease. The minimum and maximum fuel temperatures for the second fuel graphite block assemblies occurred later than the corresponding minimum and maximum temperatures of the first fuel graphite block assemblies, while the minimum and maximum temperatures of the third fuel graphite block assemblies occurred later the corresponding minimum and maximum temperatures of the first and second fuel graphite block assemblies.

It can be concluded that the bottom two layers of the fuel graphite blocks, that is CVs III to VI, start to cool down before the top layer of the fuel graphite blocks, that is CVs I and II, start to cool down. Also, the bottom two layers of the fuel graphite blocks of the third ring start to cool down before the corresponding fuel graphite blocks of

TABLE III

Fuel and Graphite Temperatures of Third Ring of Fuel Blocks of the AMR

	Fuel 3					Graphite 3				
	T_0 (°C)	T_{min} (°C)	t_{min} (s)	T_{max} (°C)	t_{max} (s)	T_0 (°C)	T_{min} (°C)	t_{min} (s)	T_{max} (°C)	t_{max} (°C)
I	404.9	365.6	107.0	428.5	30307.0	358.5	358.2	9.90	427.2	30572.0
II	599.3	424.6	1448.0	451.0	23117.0	415.9	415.5	9.37	446.4	23927.0
III	823.4	Continue decreasing				517.6	517.1	9.19	518.4	38.5
IV	965.8	Continue decreasing				629.7	629.1	9.20	629.8	24.5
V	998.4	Continue decreasing				714.6	713.9	9.38	714.1	15.7
VI	916.9	Continue decreasing				747.0	Continue decreasing			
VII	797.3	Continue decreasing				711.6	Continue decreasing			

the second ring start to cool down, which again start to cool down before the corresponding fuel graphite blocks of the first ring start to cool down. This is akin to a cooling front moving inward. In the case of the top layer of the fuel graphite blocks, the opposite trend was observed, where a heating front moved outward. The cooling of the bottom layers of the core is due to heat moving radial outward and axially upward until the full cooldown mode is reached.

III.C. HEAT/COOLING OF THE REACTOR CORE DURING DLOFC

The study of the behavior of the fuel and graphite temperatures of the first fuel graphite block assembly ring during DLOFC was augmented by considering the rates at which the CVs of the reactor core (IR to OR radially and core layer I to BR axially) were accumulating heat. The CV was heating up when the accumulation rate was positive and cooling down when the accumulation rate was negative. The time instances that were chosen were one time step before the times shown in Table I when the graphite CVs I to VI reached their maximum temperatures. The heat accumulation rates of the selected CVs are shown in Figs. 6 through 11.

The heat accumulation rates of the core CVs at t = 38.1 s, just before the temperature of graphite CV VI of the first fuel block assembly ring reached its maximum, are shown in Fig. 6. It can be observed that in correspondence with Figs. 4 and 5 and Table I, the graphite CVs I to VI of the first fuel graphite block assembly ring were heating up while the graphite CV VII was cooling down. It can also be seen in correspondence with Table I that fuel CV I was heating up and fuel CVs II to VII were cooling down. Fuel CVs II and III still had not reached their initial minimum temperatures.

It can also be seen in Fig. 6 how the various graphite and fuel CVs of the second and third fuel graphite block assembly rings were heating up or cooling down. The CVs of the IR were heating up, while CVs II to the BR of the OR were heating up and CV I was cooling down. It should be kept in mind that a large amount of heat is flowing from the graphite CVs of the third fuel graphite block assembly ring to the CVs of the OR to heat them up.

Figure 7 shows the heat accumulation rates of the core CVs at t = 93.8 s, just before the temperature of graphite CV V of the first fuel graphite block assembly ring reached its maximum. The temperature of graphite CV VI was past its maximum, and the CV was cooling

(a)	IR	GR1	FU1	GR2	FU2	GR3	FU3	OR
I	0.082	5.591	0.000	8.813	-0.026	11.871	-0.124	-0.871
II	0.500	14.732	-0.732	20.633	-1.120	18.985	-2.364	22.967
III	1.004	18.150	-1.146	23.058	-1.757	0.707	-3.765	57.032
IV	1.569	14.619	-1.020	15.434	-1.609	-37.851	-3.650	91.116
V	1.963	7.604	-0.700	3.723	-1.148	-78.083	-2.848	116.042
VI	1.912	0.017	-0.378	-8.413	-0.656	-109.699	-1.893	126.937
VII	0.877	-5.731	-0.117	-17.101	-0.245	-108.881	-0.990	133.962
BR	3.319	-6.191		-7.137		-71.680		69.437

Fig. 6. Heat accumulation rates (kJ/s) of core CVs at t = 38.1 s.

(b)	IR	GR1	FU1	GR2	FU2	GR3	FU3	OR
I	0.210	5.164	0.007	8.333	0.003	9.919	-0.010	-0.233
II	0.731	7.656	-0.091	10.974	-0.150	-0.837	-0.362	22.931
III	1.412	6.767	-0.105	7.906	-0.176	-29.632	-0.495	55.774
IV	2.164	3.946	-0.076	2.512	-0.133	-64.537	-0.487	88.610
V	2.694	0.004	-0.055	-3.753	-0.096	-94.485	-0.465	112.598
VI	2.617	-3.974	-0.040	-10.836	-0.069	-114.848	-0.435	122.924
VII	1.248	-6.687	-0.018	-17.863	-0.035	-109.012	-0.218	129.611
BR	3.006	-5.815		-8.263		-68.189		65.517

Fig. 7. Heat accumulation rates (kJ/s) of core CVs at t = 93.8 s.

down along with graphite CV VII. The graphite CVs I to V were all still heating up. Fuel CV I was still the only fuel CV of the first fuel graphite block assembly ring heating up, while fuel CVs II to VII were still cooling down. Again, it can be observed in Fig. 7 how the various graphite and fuel CVs of the second and third fuel graphite block assembly rings were heating up or cooling down. The CVs of the IR were still heating up, while CVs II to the BR of the OR were also still heating up and CV I was still cooling down.

The heat accumulation rates of the core CVs at t = 627 s, just before the temperature of graphite CV IV of the first fuel graphite block assembly ring reached its maximum, are shown in Fig. 8. The temperature of graphite CV V was now past its maximum, and it was cooling down along with the graphite CVs VI and VII. The graphite CVs I to IV were all still heating up. The temperatures of the fuel CVs II and III were now past their initial minima, and thus, fuel CVs I to III of the first fuel graphite block assembly ring were all now heating up, while the fuel CVs IV to VII were all still cooling down. Again, it can be observed in Fig. 8 how the various graphite and fuel CVs of the second and third fuel graphite block assembly rings were heating up or cooling down. The CVs of the IR were still heating up, while all the CVs of the OR were now heating up.

Figure 9 shows the heat accumulation rates of the core CVs at t = 1748 s, just before the temperature of graphite CV III of the first fuel graphite block assembly ring reached its maximum. The temperature of graphite CV IV was now past its maximum, and the CV was cooling down along with graphite CVs V to VII. The graphite CVs I to III were all still heating up. The temperature of fuel CV III was now past its maximum and was now cooling down along with fuel CVs IV to VII. The fuel CVs I and II were still heating up. It can be observed in Fig. 9 how the graphite and fuel CVs I and II of the second and third fuel graphite block assembly rings were still heating up, while all the other graphite and fuel CVs were cooling down. CVs I to IV of the IR were still heating up, while CVs V to the BR were now cooling down. All the CVs of the OR were still heating up.

The heat accumulation rates of the core CVs at t = 17 257 s, just before the temperature of graphite CV II of the first fuel graphite block assembly ring reached its maximum, are shown in Fig. 10. The temperature of graphite CV III was now past its maximum and it was cooling down along with the graphite CVs IV to VII. Graphite CVs I and II were all still heating up. The temperature of fuel CV II was now past its maximum and was now cooling down along with fuel CVs III to VII. Fuel CV I was still heating up. It can be observed in Fig. 10 how the graphite and fuel CVs I and II of the second and third fuel graphite block assembly rings

(c)	IR	GR1	FU1	GR2	FU2	GR3	FU3	OR
I	0.590	3.763	0.012	6.526	0.015	5.910	0.017	3.086
II	0.958	4.460	0.010	5.838	0.008	-1.681	-0.017	19.779
III	1.165	2.407	0.002	-0.845	-0.009	-21.497	-0.082	41.977
IV	1.450	0.002	-0.005	-8.104	-0.024	-44.990	-0.148	65.138
V	1.562	-2.693	-0.011	-15.077	-0.036	-65.239	-0.200	82.310
VI	1.280	-5.062	-0.016	-21.026	-0.046	-76.640	-0.228	89.141
VII	0.441	-6.911	-0.009	-25.355	-0.024	-71.943	-0.098	94.572
BR	1.088	-4.273		-14.544		-43.298		38.950

Fig. 8. Heat accumulation rates (kJ/s) of core CVs at t = 627 s.

(d)	IR	GR1	FU1	GR2	FU2	GR3	FU3	OR
I	0.480	2.499	0.008	3.923	0.009	3.534	0.011	4.722
II	0.653	2.858	0.008	3.252	0.006	2.010	0.003	15.652
III	0.330	0.004	-0.001	-4.193	-0.011	-7.490	-0.028	25.364
IV	0.067	-2.913	-0.010	-12.684	-0.029	-19.301	-0.062	36.266
V	-0.198	-5.574	-0.017	-20.251	-0.044	-29.863	-0.091	44.512
VI	-0.518	-7.590	-0.022	-24.993	-0.053	-34.950	-0.104	47.657
VII	-0.895	-9.051	-0.012	-26.999	-0.026	-33.279	-0.046	49.959
BR	-0.366	-5.002		-15.480		-19.460		15.618

Fig. 9. Heat accumulation rates (kJ/s) of core CVs at t = 1748 s.

(e)	IR	GR1	FU1	GR2	FU2	GR3	FU3	OR
I	0.013	0.083	0.000	0.215	0.000	0.411	0.001	1.335
II	-0.003	0.000	0.000	0.143	0.000	0.481	0.001	2.107
III	-0.083	-0.441	-0.001	-0.630	-0.002	-0.429	-0.002	0.577
IV	-0.194	-1.042	-0.003	-1.681	-0.004	-1.676	-0.005	-1.647
V	-0.296	-1.588	-0.005	-2.646	-0.006	-2.836	-0.009	-3.876
VI	-0.354	-1.888	-0.006	-3.186	-0.007	-3.512	-0.011	-5.384
VII	-0.403	-2.083	-0.003	-3.559	-0.004	-3.910	-0.006	-6.161
BR	-0.216	-1.087		-1.836		-1.885		-2.391

Fig. 10. Heat accumulation rates (kJ/s) of core CVs at t = 17 257 s.

were still heating up, while all the other graphite and fuel CVs were cooling down. CV I of the IR was still heating up, while CVs II to the BR were now cooling down. In the case of the OR, CVs I to III were still heating up, while CVs IV to the BR were now cooling down.

Finally, the heat accumulation rates of the core CVs at t = 24 512 s, just before the temperature of graphite CV I of the first fuel graphite block assembly ring reached its maximum, are shown in Fig. 11. The temperature of graphite CV II was now past its maximum and it was cooling down along with the graphite CVs III to VII. Graphite CV I was still heating up. The temperature of fuel CV I was now past its maximum, and thus, was cooling down along with fuel CVs II to VII.

It can be observed in Fig. 11 how the graphite and fuel CVs I of the second and third fuel graphite block assembly rings were still heating up, while all the other graphite and fuel CVs were all cooling down. All the CVs of the IR were now cooling down. In the case of the OR, CVs I and II were still heating up, while the CVs III to the BR were now cooling down. CV I of the OR reached its maximum temperature at t = 39 122 s. Approximately 18 h after the DLOFC started, the full reactor is in a full cooldown mode.

It can be observed in Figs. 6 through 11 how the upper part of the reactor core heated up, while the lower part of the reactor core was cooling down. A study[18] of the heat fluxes between adjacent CVs revealed how heat is conducted axially upward in the core to heat up the upper part of the core and conducted radially outward to cool down the reactor. The initial heating up of the OR was to reduce the heat flux from the third fuel graphite block assembly ring to the OR, which occurs under steady-state conditions, and to increase the heat flux to the CB, RPV, and RCCS to cool down the reactor. This results in the apparent cooling front moving inward in the lower part of the core. The apparent heating front moving outward in the upper part of the core was among others to facilitate the rejection of the excess heat accumulated in the solids. The combined heating and cooling processes enable the reactor to finally reach a full cooldown mode.

Although not the focus of this paper, it can be mentioned that the CB and the RPV reached maximum temperatures of 427°C and 293°C, respectively. All the steady-state and transient temperatures were below safely allowable maximum temperatures.[1] The reactor, therefore, can cool down passively while remaining safe.

V. CONCLUSIONS

A 2D axisymmetric network model of the AMR high-temperature prismatic block gas-cooled reactor was set up

(f)	IR	GR1	FU1	GR2	FU2	GR3	FU3	OR
I	-0.001	0.000	0.000	0.037	0.000	0.137	0.000	0.681
II	-0.021	-0.110	0.000	-0.137	0.000	-0.030	0.000	0.555
III	-0.068	-0.373	-0.001	-0.631	-0.002	-0.681	-0.002	-0.774
IV	-0.127	-0.703	-0.002	-1.246	-0.003	-1.488	-0.005	-2.449
V	-0.177	-0.980	-0.003	-1.768	-0.004	-2.187	-0.007	-4.010
VI	-0.203	-1.114	-0.003	-2.030	-0.005	-2.550	-0.008	-4.959
VII	-0.226	-1.201	-0.002	-2.208	-0.002	-2.753	-0.004	-5.417
BR	-0.119	-0.619		-1.125		-1.322		-2.215

Fig. 11. Heat accumulation rates (kJ/s) of core CVs at t = 24 512 s.

using the system network code Flownex SE. The model accounted for the core structures from the TR to the BS and from the IR to the RPV, including a simplified RCCS.

The steady-state results showed that the maximum fuel temperature was 1032.4°C, the maximum graphite temperature was 809.0°C, and the top of the core, on average, was 403°C colder than the bottom of the core. In the radial direction, the temperature profile was distorted by the heat transferred to the IR due to the coolant flowing around and the through the CR in the IR, and the heat transferred by the OR to the coolant flowing up the riser channels placed in the OR. During a DLOFC, the reactor, therefore, must endeavor to heat up the upper part of the reactor (core) to cool down the lower part of the reactor (core) and to set up the appropriate radial temperature gradient for the removal of the decay heat and the heat accumulated in the solids.

The thermal behavior of the reactor core during a DLOFC was studied by focusing on the fuel and graphite temperatures of the first, second, and third fuel graphite block rings, and the heat accumulation rates of the graphite CVs and central FA CVs of the first fuel graphite block assembly ring. It was shown how the temperatures of the graphite CVs, after initially dropping slightly, increased to heat up the upper part of the core, and after reaching the required temperatures, started to decrease to cool down the core. The fuel temperatures, after initially dropping sharply when the reactor was scrammed, followed the graphite temperatures to ensure that the decay heat that was generated was transferred from the fuel to the graphite. The maximum fuel temperatures reached during the DLOFC were all below the corresponding steady-state values, and all the temperatures were below the maximum allowable temperature of 1130°C.[1]

The analysis of the CV heat accumulation rates will in future be extended by adding the results of the analysis of the conduction heat transfer rates between the CVs presented by Du Toit et al.[18] These results, in combination with the analysis of the decay heat generated, the stored heat released by the solids, and the heat removed by the RCCS during the DLOFC, also presented by Du Toit et al.,[18] could lead to a thorough understanding of the thermal-hydraulic behavior of the reactor during a DLOFC.

It could be noted that during the first 20 h of the DLOFC, the stored heat released by the solids comprised 32.8% of the heat removed by the RCCS, and during the following 30 h, the stored heat comprised 42.5% of the heat removed by the RCCS.

This paper demonstrated how the methodology was applied to study the heating and cooling of the core of the current conceptual design of the AMR. The focus, in particular, was on the inner fuel ring to understand and evaluate how the heating and cooling developed with time and the relationship between the fuel and graphite temperatures during a DLOFC. The methodology also helped with the identification of the underlying phenomena that determine the behavior of the reactor during a DLOFC.

Once more detailed design information is available, the model will be refined and the upper and lower domes, cross flow, and bypass gaps, and the contact thermal conductance will be accounted for in the simulation and analysis of the reactor, making it possible to quantify the effect of the simplifying assumptions made in the current model.

Nomenclature

A = area (m^2)
c_p = specific heat (J/kg K)
D_H = hydraulic diameter (m)
d = mass source (kg/s)
F = view factor
f = friction factor
h = heat transfer coefficient (W/m^2 K)
h_0 = total enthalpy (J/kg)
K = minor loss factor
k = thermal conductivity (W/m K)
L = length (m)
m = mass of CV (kg)
$\dot{m}$ = mass flow rate (kg/s)
p = static pressure (N/m^2)
p_0 = total pressure (N/m^2)
$\dot{Q}$ = heat source (W)
$\dot{Q}_{DH}$ = decay heat (W)
$\dot{q}$ = heat transferred (W)
T = static temperature (K)
t_1 = start time of DLOFC (s)
t_2 = end time of depressurization (s)
t_s = time before scram (s)
U = velocity (m/s)
V = volume (m^3)

Greek

ε = emissivity

ρ = density (kg/m_3)

σ = Boltzmann constant (W/m^2K^4)

Superscript/subscript

0	= nominal value
∞	= ultimate value
amb	= ambient
cond	= conduction
conv	= convection
ex	= exit, outlet
f	= fluid, gas
i,j	= indices
in,out	= inlet, in; outlet, out
rad	= radiation
s	= solid
+	= added
−	= removed

Acknowledgments

The authors wish to thank the University of Pretoria and the North-West University for the opportunity to perform this study.

Disclosure Statement

No potential conflict of interest was reported by the author(s).

Author Contributions

CRediT: **Charl du Toit:** Formal analysis, Investigation, Methodology, Writing – original draft; **Wayne Boyes:** Conceptualization, Writing – review & editing; **Johan Slabber:** Conceptualization, Writing – review & editing.

ORCID

Charl du Toit http://orcid.org/0000-0003-1526-6744

References

1. W. A. BOYES et al., "Evaluation of the Basic Neutronic and Thermal-Hydraulics for the Safety Evaluation of the Advanced Micro Reactor (AMR)," *Nucl. Sci.*, **8**, *1* (2023); https://doi.org/10.11648/j.ns.20230801.13.
2. N. I. TAK et al., "Development of a Core Thermo-Fluid Analysis Code for Prismatic Gas Cooled Reactors," *Nucl. Eng. Technol.*, **46**, *5*, 641 (2014); https://doi.org/10.5516/NET.02.2014.020.
3. D. TOCHIO and S. NAKAGAWA, "Numerical Simulation of Three-Dimensional Thermal-Hydraulic Behaviour for HTTR (High Temperature Engineering Test Reactor)," *Nucl. Eng. Des.*, **241**, *5*, 1616 (2011); https://doi.org/10.1016/j.nucengdes.2011.01.032.
4. S. MARUYAMA et al., "Evaluation of Core Thermal and Hydraulic Characteristics of HTTR," *Nucl. Eng. Des.*, **152**, *1–3*, 183 (1994); https://doi.org/10.1016/0029-5493(94)90084-1.
5. P. G. ROUSSEAU and G. P. GREYVENSTEIN, "Modelling of the HTTR in Flownet," *Proc. 1st Int. Topl. Mtg. on High Temperature Reactor Technology (HTR-TN 2022)*, p. 318, Petten, Netherlands, April 22–24, 2002, European Nuclear Society (2002).
6. N. ANDERSON, Y. HASSIN, and R. SCHULTZ, "Analysis of the Hot Gas Flow in the Outlet Plenum of the Very High Temperature Reactor Using Coupled RELAP5-3D System Code and a CFD Code," *Nucl. Eng. Des.*, **238**, *1*, 274 (2008); https://doi.org/10.1016/j.nucengdes.2007.06.008.
7. M. H. KIM, N. I. TAK, and H. S. LIM, "Thermal-Fluid Assessment of the Design Options for Reactor Vessel Cooling in a Prismatic Core VHTR," *Ann. Nucl. Energy*, **37**, *12*, 1774 (2010); https://doi.org/10.1016/j.anucene.2010.08.007.
8. G. J. NEL, "Simulation of the Heat Transfer and Coolant Flow for a PMR200 Reactor Using a Network Approach in Flownex," PhD Thesis, North-West University, Unit for Energy and Technology Systems (Nov. 2022).
9. "Flownex Simulation Environment," Version8.16.0.5518, M-TECH Industrial (2024); http://www.flownex.com (accessed June 8, 2025).
10. J. P. SIMONEAU et al., "Three-Dimensional Simulation of the Coupled Convective, Conductive, and Radiative Heat Transfer During Decay Heat Removal in an HTR," *Nucl. Eng. Des.*, **237**, *15–17*, 1923 (2007); https://doi.org/10.1016/j.nucengdes.2007.03.010.
11. L. J. LOMMERS, B. E. MAYS, and F. SHAHROKHI, "Passive Heat Removal Impact on AREVA HTR Design," *Nucl. Eng. Des.*, **271**, 569 (2014); https://doi.org/10.1016/j.nucengdes.2013.12.034.
12. V. L. STREETER and E. B. WYLIE, *Fluid Mechanics*, 7th ed. p. 239, McGraw-Hill, Tokyo, Japan (1979).

13. F. P. INCROPERA and D. P. DEWITT, *Fundamentals of Heat and Mass Transfer*, 4th ed. p. 445, John Wiley & Sons, New York (1996).

14. W. J. GARLAND and F. SAUNDERS, "Decay Heat Estimates for MNR," Technical Report 1998-05, McMaster University (1998).

15. P. G. ROUSSEAU et al., "Code-to-Code Comparison for Analysing the Steady-State Heat Transfer and Natural Circulation in an Air-Cooled RCCS Using GAMMA+ and Flownex," *Nucl. Eng. Des.*, **291**, 71 (2015); https://doi.org/10.1016/j.nucengdes.2015.05.004.

16. G. P. GREYVENSTEIN, "An Implicit Method for the Analysis of Transient Flows in Pipe Networks," *Int. J. Numer. Meth. Eng.*, **53**, *5*, 1127 (2002); https://doi.org/10.1002/nme.323.

17. C. G. DU TOIT, "1D Network Modelling of a VHTR Prismatic Block Fuel Assembly," *Proc. 17th Int. Heat Transfer Conf. (IHTC-17)*, Paper 0122, Cape Town, South Africa, August 14–18, 2023 (2023).

18. C. G. DU TOIT, W. A. BOYES, and J. F. M. SLABBER, "Thermal-Hydraulic Behaviour of a Micro Nuclear Reactor During a DLOFC Transient," *Proc. 13th SA Conf on Computational and Applied Mechanics (SACAM 2024)*, p. 50, Stellenbosch, South Africa, January 22–23, 2024 (2024).